Influence of a Top Crust of Entangled Nanotubes on the Structure of Vertically Aligned Forests of Single-Walled Carbon Nanotubes

Liang Zhang,[†] Zhongrui Li,[†] Yongqiang Tan,[†] Giulio Lolli,[†] Nataphan Sakulchaicharoen,[†] Félix G. Requejo,[‡] B. Simon Mun,[§] and Daniel E. Resasco*[,†]

School of Chemical, Biochemical, and Materials Engineering, University of Oklahoma, Norman, Oklahoma 73019, Departamento de Física and INIFTA-IFLP (CONICET), Universidad Nacional de La Plata, 1900 La Plata, Argentina, and Lawrence Berkeley National Laboratory, Berkeley, California 94720

Received July 30, 2006. Revised Manuscript Received September 6, 2006

The time evolution of the growth process of vertically aligned single-walled carbon nanotubes (or V-SWNTs) on a flat substrate was examined by scanning electron microscopy (SEM), resonant Raman spectroscopy, and angle-resolved X-ray absorption near-edge structure (XANES). This detailed characterization gives evidence for the growth of a thin layer (crust) of randomly oriented single-walled carbon nanotubes during the first stages of the growth process. This crust is responsible for the unique forest-like morphology exhibited by this type of SWNT structure.

1. Introduction

Despite large uncertainties in the measurements and differences in the synthesis methods employed, it is well-recognized that, in an unrestricted state, the growth rate of single-walled carbon nanotubes is at least higher than several micrometers per second.[1−4] By contrast, when the growth occurs via catalytic decomposition of carbon-containing molecules on high surface area catalysts, such as CoMo/SiO_2, the growth takes place in a scale of hours. As previously proposed,[5] while the amount of carbon deposits slowly increases with time, this does not necessarily mean that the growth of a given nanotube is so slow. It is plausible that the slow rate observed for the overall rate of carbon deposition is in fact a slow rate of nucleation followed by a fast nanotube growth rate. Accordingly, new nucleation sites will appear on a high surface area material and each site will give rise to a nanotube that grows relatively fast. Of course, the nanotubes that grow later will do it constricted by the presence of those that grew earlier. As a result, control of nanotube length during growth appeared as an almost impossible task for a long time. However, recent studies of SWNT growth on flat substrates have shown that, in fact, the length of SWNTs can be controlled.[6−13] In our previous contribution,[14] we indicated that the density and distribution of the catalyst moieties on the flat surface is crucial to determine whether the nanotubes grow in a vertically oriented fashion ("forest" or V-SWNTs) or a random network parallel to the surface ("grass"). We found that different forms of SWNT arrays can be reproducibly obtained on flat silicon substrates when the Co−Mo catalyst particles have the appropriate distribution, which can be readily controlled by simply varying the concentration of catalyst solution.[14]

The difference between this type of flat catalyst and the high surface area catalyst is that on a flat surface the nanotube growth is, in principle, less constricted by the catalyst structure due to the absence of porosity. However, the growth of a nanotube is still constricted by the presence of the other nanotubes, which as we will show make them grow vertically oriented (V-SWNTs). A question that remains unanswered is why all the SWNTs that form the "forest" appear to have the same length and what is most puzzling is the smoothness of the top of the forest clearly observed in the SEM images.[7,14]

In this contribution, we have investigated in detail the structure of the forest and, from this analysis, we attempt to elucidate the way in which these forests are formed. To characterize the forest, we have used angle-resolved X-ray

* Corresponding author. E-mail: resasco@ou.edu. Phone: 405-325-4370. Fax: 405-325-5813.
[†] University of Oklahoma.
[‡] Universidad Nacional de La Plata.
[§] Lawrence Berkeley National Laboratory.

(1) Puretzky, A. A.; Schittenhelm, H.; Fan, X.; Lance, M. J.; Allard, L. F., Jr.; Geohegan, D. B. *Phys. Rev. B* **2002**, *65*, 245425.
(2) Gorbunov, A. A.; Friedlein, R.; Jost, O.; Golden, M. S.; Fink, J.; Pompe, W. *Appl. Phys. A* **1999**, *69*, S593.
(3) Arepalli, S.; Nikolaev, P.; Holmes, W.; Files, B. S. *Appl. Phys. Lett.* **2001**, *78*, 1610.
(4) Scott, C. D.; Arepalli, S.; Nikolaev, P.; Smalley, R. E. *Appl. Phys. A* **2001**, *72*, 573.
(5) Alvarez, W. E.; Pompeo, F.; Herrera, J. E.; Balzano, L.; Resasco, D. E. *Chem. Mater.* **2002**, *14*, 1853.
(6) Zhong, G. F.; Iwasaki, T.; Honda, K.; Furukawa, Y.; Ohdomari, I.; Kawarada, H. *Chem. Vap. Deposition* **2005**, *11*, 127.
(7) Maruyama, S.; Einarsson, E.; Murakami, Y.; Edamura, T. *Chem. Phys. Lett.* **2005**, *403*, 320.
(8) Hata, K.; Futaba, D. N.; Mizuno, K.; Namai, T.; Yumura, M.; Iijima, S. *Science* **2004**, *306*, 1362.
(9) Murakami, Y.; Chiashi, S.; Miyauchi, Y.; Hu, M.; Ogura, M.; Okubo, T.; Maruyama, S. *Chem. Phys. Lett.* **2004**, *385*, 298.
(10) Hu, M.; Murakami, Y.; Ogura, M.; Maruyama, S.; Okubo, T. *J. Catal.* **2004**, *225*, 230.
(11) Murakami, Y.; Einarsson, E.; Edamura, T.; Maruyama, S. *Carbon* **2005**, *43*, 2664.
(12) Futaba, D. N.; Hata, K.; Yamada, T.; Mizuno, K.; Yumura, M.; Iijima, S. *Phys. Rev. Lett.* **2005**, *95*, 056104.
(13) Futaba, D. N.; Hata, K.; Namai, T.; Yamada, T.; Mizuno, K.; Hayamizu, Y.; Yumura, M.; Iijima, S. *J. Phys. Chem. B* **2006**, *110*, 8035.
(14) Zhang, L.; Tan, Y.; Resasco, D. E. *Chem. Phys. Lett.* **2006**, *422*, 198.

10.1021/cm061783b CCC: $33.50
Published on Web 10/18/2006

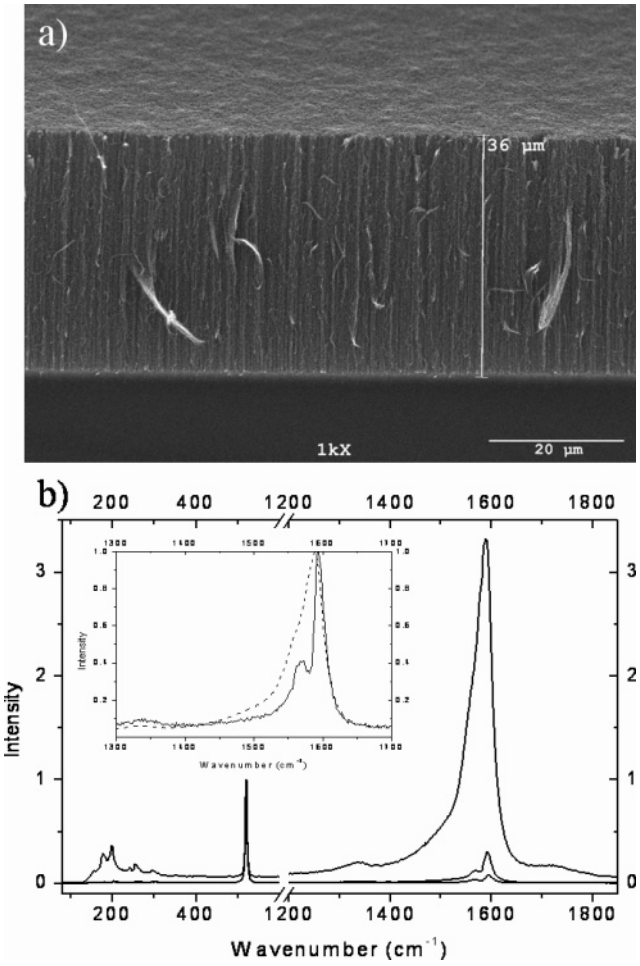

Figure 1. SEM image (a) and Raman spectra (b) of a forest of V-SWNTs obtained on CoMo/Si flat substrate by decomposition of CO at 750 °C. Raman spectra of V-SWNTs were obtained for a series of reaction time periods: 0.5, 3, and 10 min from bottom to top. These three curves are normalized with respect to the Si band at 520 cm^{-1}. The inset is the G band of V-SWNTs obtained for 0.5 min (solid line) and 10 min (dashed line) respectively when normalized with respect to the G band.

absorption, SEM, and Raman spectroscopy. The X-ray absorption near-edge structure (XANES) technique involves the excitation of electrons from a core shell (in our case C(1s)) to unfilled states. The peak positions and spectral line shape in a XANES spectrum are directly associated with the nature of these unoccupied electronic states. Accordingly, XANES can be used to obtain qualitative bonding information for a full range of the sp^2/sp^3 bonding ratios.[15] It can be used to identify specific bonds in molecules (e.g., C═C, C−C, and C−O bonds) as well as the presence of chemisorbed species.[16] Of greater importance for this study, by using a linearly polarized X-ray beam, angle-dependent XANES can be used to investigate the angular dependence of the specific orbitals involved in the transition 1s → π^* and 1s → σ^*. In addition to XANES we have used Raman and SEM to evaluate the nature and morphology of the V-SWNTs produced on Co−Mo catalysts. The characterization results give evidence for the presence of a crust of entangled nanotubes on top of the forest that shapes the morphology of the entire forest and constricts the nanotubes to grow to the same length.

2. Experimental Section

2.1. Production of V-SWNT on Co−Mo/Si Substrates. Catalyst solutions of Co and Mo were prepared as described elsewhere.[14] A drop of catalyst solution was deposited on a p-type Si wafer, with a SiO_2 layer of 300 nm obtained from Montco Silicon Technologies, Inc. After deposition, the wafer was placed in a covered Petri dish to allow for a slow drying of the impregnating solution. This slow-drying method results in a uniform catalyst film. Following the drying step, the wafer containing the catalyst film was baked in a convection oven at 100 °C for 10 min and then calcined at 500 °C for 15 min. After this pretreatment, the wafer was placed in a quartz reactor, oriented parallel to the direction of the flowing gas. Prior to the production of SWNT by CO disproportionation reaction, the catalyst was heated in H_2 flow from room temperature to 500 °C, and then in He flow up to 750 °C. The flow rate was kept at 1000 sccm for both gases. Subsequently, the flow of pure CO at a rate of 1000 sccm was initiated to conduct the nanotube growth at atmospheric pressure. The resulting carbon structure is illustrated in the SEM image of Figure 1a. As shown in the previous study, both Raman and TEM demonstrate that all the nanotubes are SWNTs.

2.2. Characterization of V-SWNTs. The as-produced SWNTs over the catalyst/wafer were characterized by angle-resolved X-ray near-edge structure spectroscopy (XANES), Raman spectroscopy, and electron microscopy (SEM and TEM). The angle-dependent C *K*-edge XANES spectra were taken under UHV with total electron yield (TEY) mode at the bending magnet beamline 9.3.2 of Advanced Light Source (ALS) in Lawrence Berkeley National Laboratory (LBNL). The XANES data were collected at various angles ranging from $\theta = 10°$ ("glancing geometry") to $\theta = 80°$ ("normal geometry"), where θ denotes the angle between the sample normal and the direction of the electric vector of the X-ray beam. The Raman spectra were obtained in a Jovin Yvon-Horiba Lab Ram equipped with a charge coupled detector. The SEM images were obtained in a JEOL JSM-880 high-resolution scanning electron microscope, while the TEM studies were conducted on a JEOL JEM-2000FX transmission electron microscope.

Results and Discussion

In addition to SEM (Figure 1a) and TEM, resonant Raman spectroscopy (Figure 1b) with 633 nm laser as excitation energy was used to characterize the nature of the nanotubes grown on the flat substrate. All the Raman spectra observed on these samples are consistent with SWNTs. From very short contact times to more than 30 min of reaction time, the Raman spectra display an intense G band at 1590 cm^{-1}, a very weak D band at 1340 cm^{-1}, and radial breathing mode bands in the range 150−300 cm^{-1}, typical of SWNTs of high quality. In addition to the SWNT bands, a sharp peak at 520 cm^{-1}, characteristic of silicon, is clearly observed. Obviously, the intensity of this band relative to that of the carbon G band decreases with the height of the V-SWNTs covering the substrate; this decrease is due to both the increasing amount of carbon absorbing laser radiation as well as the change in the focal plane away from the Si surface as the forest grows.

Figure 2a shows the changes in the XANES spectra of the 30-μm long SWNT forest for different incident angles

(15) Coffman, F. L.; Cao, R.; Pianetta, P. A.; Kapoor, S.; Kelly, M.; Terminello, L. *J. Appl. Phys. Lett.* **1996**, *69*, 568.
(16) Stohr, J. In *NEXAFS Spectroscopy*; Springer-Verlag: Berlin, 1992.

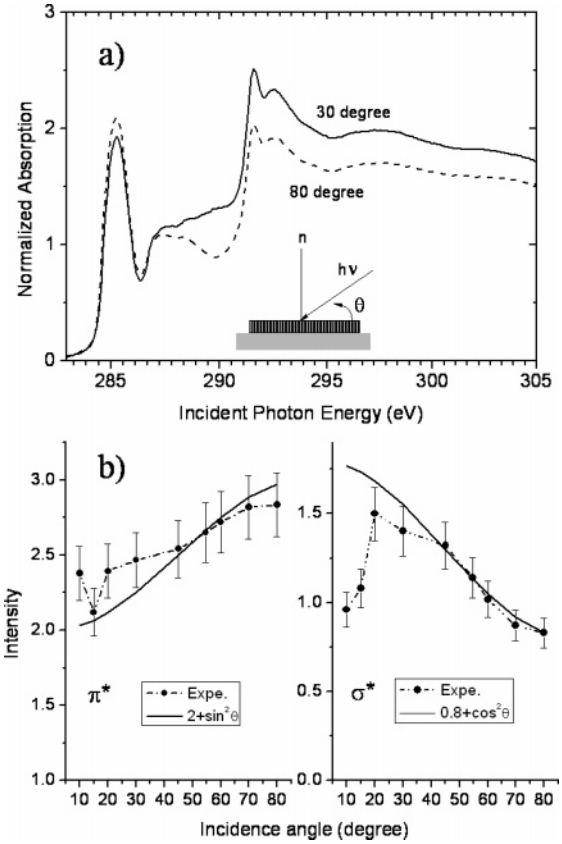

Figure 2. (a) XANES spectra of V-SWNTs (30 μm) at different angles with respect to the top surface of V-SWNTs; (b) experimental and fitted data of σ^* and π^* peak intensity.

θ, which is also the angle between the axis of the vertical nanotubes and the electric field vector of the X-ray beam. In all the spectra, the pre-edge and post-edge regions were normalized to 0 and 1, respectively. Several characteristic peaks can be identified at the C *K*-edge which is similar to that of graphite,[17] and has been previously discussed.[18] The spectra are characterized by a sharp C(1s)-to-π^* transition near 285.4 eV, a sharp C(1s)-to-σ^* transition near 291.5 eV, two other σ^* transitions from 292 to 298 eV, and broader ($\sigma + \pi$) transitions between 301 and 309 eV. The position and width of these resonances are typical of C−C single bonds.[19] Two smaller peaks in the 287−290 eV region can be assigned to oxygenated surface functionalities, perhaps associated with a small level of defects of the nanotubes. According to Kunetsova et al.,[20] these peaks would correspond to π^* C═O and σ^* C−O resonances.

Following the method proposed by Outka and Stohr,[21] the XANES spectra were fitted to an arctangent step corresponding to the excitation edge of carbon, a smooth decreasing background, and a series of Gaussians,. The fitting program EDG_FIT by G. N. George, SSRL, available from http://ssrl.slac.stanford.edu/exafspak.html, which utilizes the double-precision version of the public domain MINPAK fitting library,[22] was used for the fit. All spectra were fit over the range of 275−325 eV. Pseudo-Voigt line shapes of a fixed 1:1 ratio of the Lorentzian to Gaussian contribution were used to model the π^* and σ^* resonances features and successfully reproduce the spectra. Functions modeling the background contributions to the pre-edge features were chosen empirically to give the best fit and included pseudo-Voigt functions that mimicked shoulders on the rising edge. For all spectra, a fit was considered acceptable only if it successfully reproduced the data as well as the second derivative of the data. The resonance peak area after the background subtraction was obtained by integrating over a range of 10 eV.

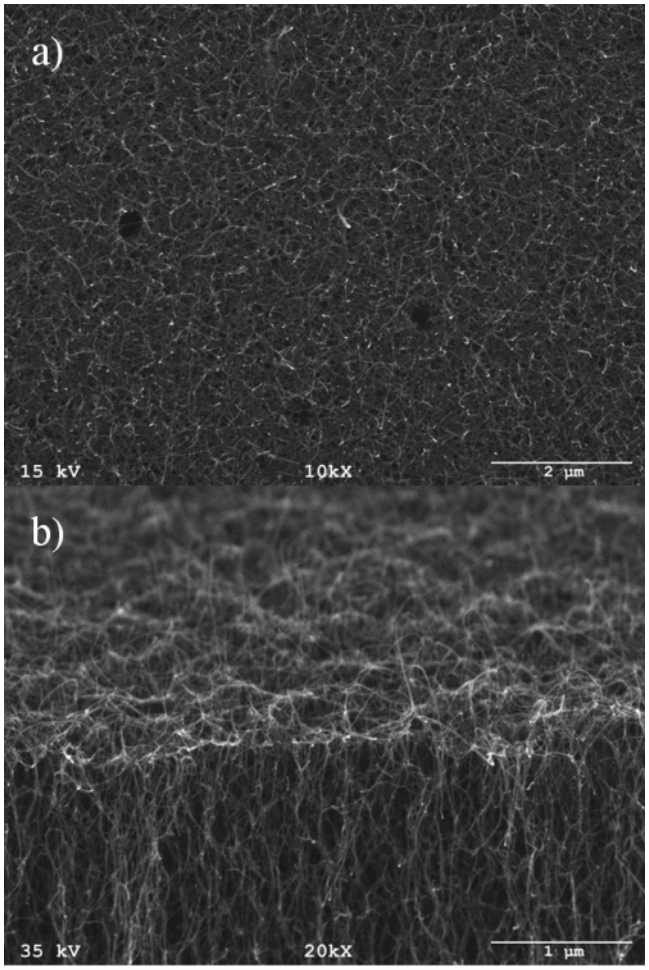

Figure 3. Top (a) and 60° (b) views of a typical V-SWNT sample observed by SEM.

The local order of the SWNTs is clearly evident in the angular dependence of the XANES series. Since the synchrotron light is linearly polarized horizontally, the intensity of the π^* transition is sensitive to the orientation of the π^* orbital with respect to the polarization vector. Thus, since the π^* orbitals in the nanotube specimen are oriented with respect to the incident photon beam, a rotation of the specimen with respect to the incoming photon shows a measurable angular dependence. At normal incidence, the

(17) Skytt, P.; Glans, P.; Mancini, D. C.; Guo, J.-H.; Wassdahl, N.; Nordgren, J.; Ma, Y. *Phys. Rev. B* **1994**, *50*, 10457.
(18) Banerjee, S.; Hemraj-Benny, T.; Balasubramanian, M.; Fischer, D. A.; Misewich, J. A.; Wong, S. S. *ChemPhysChem* **2004**, *5*, 1416.
(19) Sette, F.; Stohr, J.; Hitchcock, A. P. *J. Chem. Phys.* **1984**, *81*, 4906.
(20) Kuznetsova, A.; Popova, I.; Yates, J. T., Jr.; Bronikowski, M. J.; Huffman, C. B.; Liu, J.; Smalley, R. E.; Hwu, H. H.; Chen, J. G. *J. Am. Chem. Soc.* **2001**, *123*, 10699.
(21) Outka, D. A.; Stohr, J. *J. Chem. Phys.* **1988**, *88*, 3539.
(22) More, J. J.; Garbow, B. S.; Hillstrom, K. E. *ACM Trans. Math. Software* **1981**, *7*, 17.

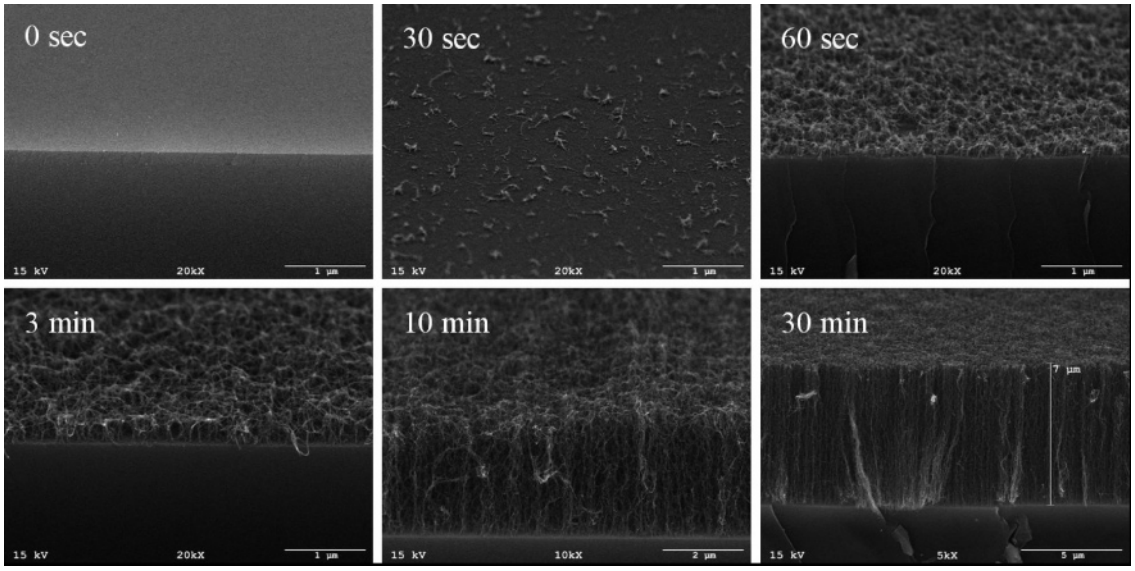

Figure 4. SEM images of V-SWNTs obtained for a series of reaction time periods. The scale bars in those images are 1 μm for 0 s, 30 s, 60 s, and 3 min, 2 μm for 10 min, and 5 μm for 30 min.

electric field **E** is in the same cross-section plane as the π^* orbitals, and thus, the π^* resonance peak is the highest at this angle, as opposed to at glancing angles. Conversely, when **E** is normal to the surface, the field lies along the tube axis (along *z*) and is perpendicular to the plane of the π^* orbitals; the intensity of the π^* resonance is at its minimum. Specifically, there is an increase in the intensity of the π^* resonance with increasing angle of X-ray beam incidence. The local contribution to the π^* excitation XAS intensity is proportional to the square of the scalar product of the local normal and **E.** As shown before, the π^* resonance intensity is proportional to the sine-squared function of the incidence angle. Indeed, a plot of the π^* excitation vs the incidence angle shows an approximate sine-squared dependence, as shown in the left panel of Figure 2b. By contrast, a C−C σ^* orbital orthogonal to the π^* orbital should show an opposite trend. The σ^* orbitals can be viewed as a combination of two perpendicular components: one is parallel to the tube axis direction ($\sigma^*_{||}$) and another along the circumferential direction (also perpendicular to the tube axis, $\sigma^*_{\perp}$). The local contribution to the σ^* excitation XAS intensity at 291.5 eV is proportional to the sum of the squared scalar products of the two components and electric polarization vector. With a simple calculation by accounting for all σ^* contributions on the entire tube circumference, we found the intensity of the σ^* bound resonance at 291.5 eV is indeed roughly proportional to $(0.8 + \cos^2\theta)$,[23] as shown in Figure 2b. However, deviations from the predicted trend are observed for both σ^* and π^* transition at low angles. These deviations are consistent with a fraction of the tubes, most noticeable at grazing angles, oriented parallel to the surface, rather than perpendicular as the majority of the tubes in the forest.

In fact, a closer inspection of the top of the forest reveals the presence of SWNTs oriented parallel to the surface (Figure 3a). However, only the very top layer of the forest has the nanotubes with parallel orientation. Immediately below this top layer (crust), the orientation is preferentially vertical (Figure 3b). Maruyama et al.[7] and Xu et al.[24] have shown similar SEM images that evidence the presence of a disordered structure on top of the forest.

To investigate how this crust develops during the growth process, we have followed the evolution of the forest structure as a function of time. Figure 4 clearly shows the different morphologies of the nanotube layer observed as a function of time. The first image shows the flat catalyst surface before any carbon was deposited. Next, the appearance of short SWNTs is observed after only 30 s. of reaction time. It is evident that the early growth does not occur over the entire surface, but rather on some preferential spots which are those in which the development of the active Co−Mo catalyst and nucleation of nanotube caps occurs first, as proposed earlier.[5,14] It is important to note that during the early stages of the growth process, there is no indication of a vertically oriented structure. During the following 30 s, it appears that the entire surface has been covered by nanotubes, with evidence of sites being activated at a later time than the first ones. As a result, a thin layer of randomly oriented SWNTs gets woven. After 3 min, a uniform crust with very short aligned SWNT bundles underneath can be clearly seen. This is a critical moment. It is obvious that the entangling of SWNT bundles due to different growth rates and random orientations has stopped at this stage; instead, as the nanotube growth continues from the root, the crust is pushed up, but being rather rigid, the overall growth is now concerted. Consequently, a microscopically uniform growth is forced and a somewhat vertical alignment of every nanotube occurs.

Figure 5a illustrates with greater detail the relative rigidity of the crust, which remains connected while, in this case, a piece has become detached from the rest of the forest. The higher brightness of the crust is due to a higher intensity of secondary electrons emitted by the crust, which is much

(23) Banerjee, S.; Hemraj-Benny, T.; Sambasivan, S.; Fischer, D. A.; Misewich, J. A.; Wong, S. S. *J. Phys. Chem. B* **2005**, *109*, 8489.

(24) Xu, Y. Q.; Flor, E.; Kim, M. J.; Hamadani, B.; Schmidt, H.; Smalley, R. E.; Hauge, R. H. *J. Am. Chem. Soc*. **2006**, *128*, 6560.

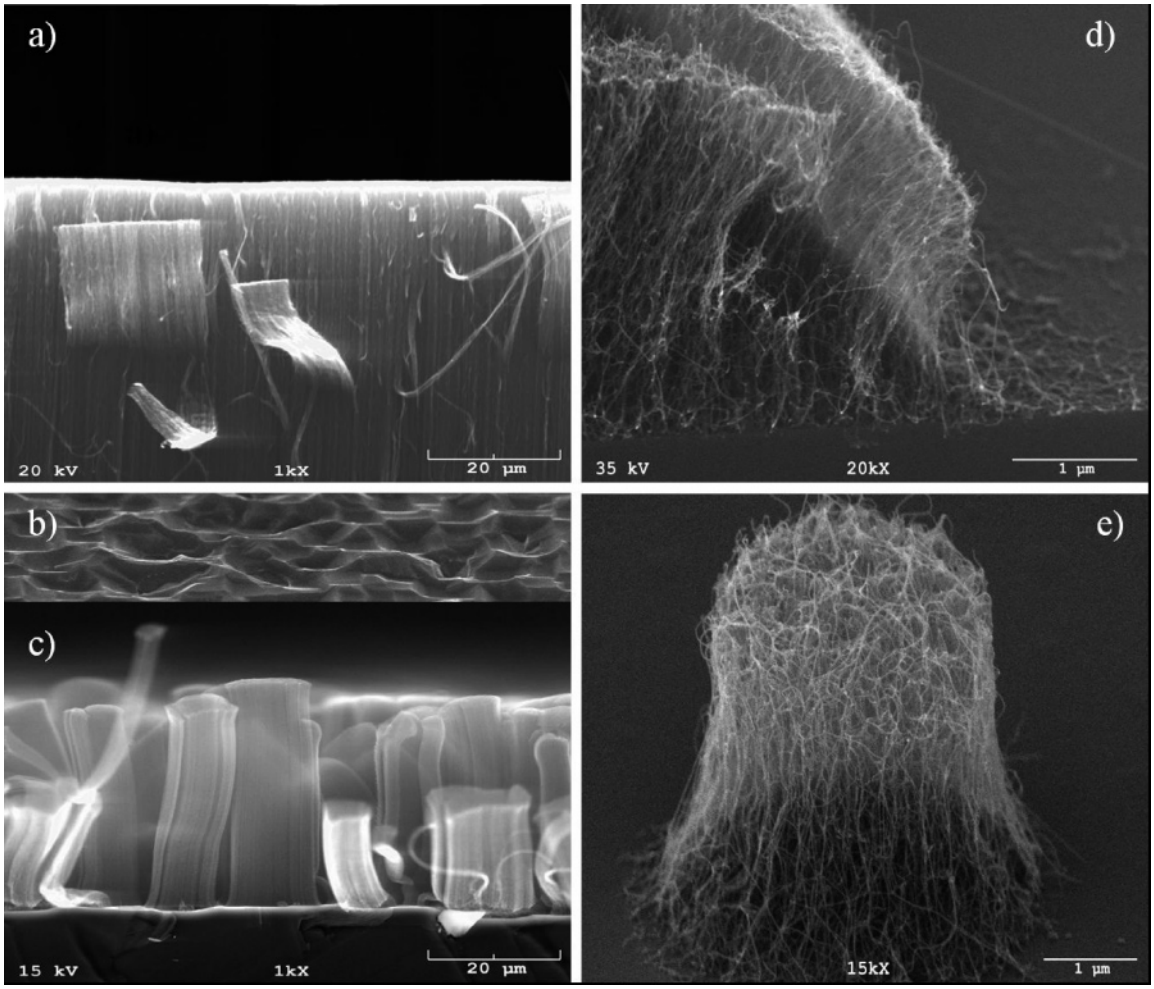

Figure 5. SEM image of V-SWNTs grown on (a) a flat silicon wafer surface, (c) a rough silicon wafer surface, (d) end of a region covered with nonuniform distribution of catalyst, and (e) a small circular spot covered with catalyst on a bare silicon surface. (b) is a rough silicon wafer surface after deposition of Co−Mo catalyst.

denser than the rest of the forest. As indicated in previous work, electron diffraction of the crust region showed the total absence of any metal. As mentioned by previous authors,[8,14] the forest-type growth occurs at the root and all of the metal remains on the substrate.

Further demonstrations of the role of the crust in determining the structure of the resulting forest have been obtained by depositing the Co−Mo catalyst in a nonuniform manner over the flat substrate. For example, when the catalyst was deposited on the rough surface side of the silicon wafer, instead of obtaining a uniform catalyst film, the catalyst preferentially deposited on the shallow depressions of the unsmooth surface (see Figure 5b). As a result, the nanotube growth occurred on separate domains, with each domain generating a separate crust. Therefore, the height and orientation of each domain were somewhat different, as illustrated in Figure 5c. The curvature of the top of the crust in these small domains contrasts with the much flatter surface observed on the broader area forests, for which the effects of the edges is less pronounced. One can imagine that when the crust is pushed away from the surface as the nanotube growth proceeds, the edges will be unevenly pushed up, which causes the curvature. To investigate the effects of the edges on the forest, we prepared samples in which the catalyst was only deposited on certain regions. For example, the effect of the edge is illustrated in Figure 5d, which shows the separation between a region with catalyst and the bare substrate. It can be seen that the entangled crust is resting on the substrate at the border where no catalyst is present, this interaction with the substrate anchors the whole crust, and the nanotubes growing beneath make the crust curve. Similarly, Figure 5e shows the case in which the use of a very fast drying rate produced circular spots of dried catalyst. The small size of these islands (roughly 4 μm in diameter) and nonuniformity of catalyst distribution make the edge effect more pronounced.

Conclusions

A detailed analysis of the structure of SWNT forests as a function of growth time reveals that a two-step process is responsible for the formation of a SWNT forest. The first step is the weaving of a crust of entangled SWNTs which grow at different rates and with random orientation over the surface. The second step is a concerted growth of vertically aligned SWNTs constrained by the uniform top crust. Several techniques were employed to examine the growth process and the results are all consistent with this mechanism. The XANES results show that a fraction of the tubes on top of the forest are parallel to the surface, rather than perpendicular as the majority of the tubes in the forest. Direct SEM

observations agree with this morphology. Several examples are presented to demonstrate that the crust influences the morphology of the resulting forest. Catalysts which are nonuniformly distributed on the substrate produce curved crusts instead of the consistent forest with a flat top obtained when the catalyst layer is uniform.

Acknowledgment. This work is part of the Carbon Nanotube Technology Center Program (funded by DoE under DE-FG02-06ER64239). We gratefully acknowledge the financial support from the Department of Energy (Grant DE-FG03−02.ER15345) and from the National Science Foundation (Grant No. CTS-0308619). We also thank Preston Larson for his kind assistance in SEM measurement and the personnel at the Lawrence Berkeley National Laboratory for their help in XANES measurement.

CM061783B